Generalized Analysis of Microstrip-Like Transmission Lines and Coplanar Strips With Anisotropic Substrates for MIC, Electrooptic Modulator, and SAW Application

SHIBAN KISHEN KOUL, STUDENT MEMBER, IEEE,
AND BHARATHI BHAT, SENIOR MEMBER, IEEE

Abstract—A unified variational expression is presented for the line capacitance of a general, multilayer anisotropic structure. The propagation characteristics of a variety of striplines, microstriplines, and coplanar strips, in isolated and coupled configurations, with anisotropic substrates having optical axis aligned along the axis of the substrate, are computed. The characteristics of these structures with anisotropic substrates having tilted optical axis are also studied. Using the formulas presented, the study of structures with anisotropic substrates having aligned or tilted optical axis, for various applications including MIC, electrooptic modulator, and SAW IDT, reduces to the determination of a single admittance parameter. This parameter can be obtained from the transmission-line equivalent circuit of the structure almost by inspection.

I. Introduction

THE MOST COMMONLY used planar transmission lines for MIC application are i) single conductor transmission line (Fig. 1(a)), ii) edge-coupled transmission line (Fig. 1(b)), iii) broadside-coupled transmission line (Fig. 1(c)), and iv) broadside, edge-coupled transmission line (Fig. 1(d)). The conventional stripline and microstripline, in isolated and coupled configurations, on isotropic substrates have been extensively analyzed [1]. The isotropic substrates commonly used are RT duroid, alumina, and fused quartz. Some anisotropic substrates, e.g., sapphire and pyrolytic boron nitride, have certain advantages over ceramics, which include lower losses, higher homogeneity, and lower variations of electrical properties from specimen to specimen [2]–[3]. The analysis of conventional stripline and microstripline, in isolated and coupled configurations, with uniaxial anisotropic substrates, are reported in several papers [4]–[5]. Recently, the propagation characteristics of isolated stripline and edge-coupled microstripline with anisotropic substrates having tilted optical axis have been reported [6]–[7]. It has been shown that by varying the angle of tilt, the even- and odd-mode phase velocities in the case of edge-coupled microstriplines can be equalized.

There are several other strip and microstrip-like transmission lines reported in the literature, namely, suspended stripline, stripline-like microstrip, double-layer microstrip, suspended microstrip, microstrip with overlay, and inverted microstrip, which offer specific advantages over the conventional strip and microstriplines. Except for the inverted microstrip and suspended microstrip [8]–[9], the study of the propagation parameters of these transmission lines, in isolated and coupled configurations, has been confined only to the isotropic dielectric case. Further, the analysis of various strip and microstrip-like transmission lines with anisotropic substrates having tilted optical axis has not been attempted so far.

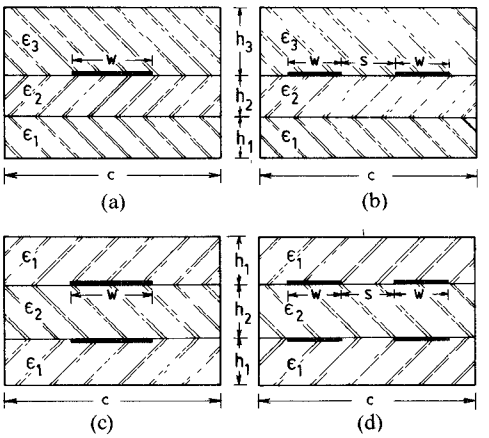

Fig. 1. A schematic of (a) single conductor transmission line, (b) edge-coupled transmission line, (c) broadside-coupled transmission line, and (d) broadside, edge-coupled transmission line.

A typical surface acoustic-wave (SAW) device uses an interdigital transducer deposited on nonpiezoelectric substrate. A thin film of piezoelectric material is placed on top of the transducer in good acoustic contact with it, and a metal film may be deposited on top of the piezoelectric film. Typical examples of the materials which are used are Zno, Cds, or $LiNbo_3$ for the piezoelectric layer and Si, sapphire, and fused silica for the nonpiezoelectric substrate. Most of these materials exhibit anisotropic behavior. Following certain assumptions [10], the determination of the static capacitance of a surface acoustic-wave interdig-

Manuscript received March 25, 1983; revised August 16, 1983.

The authors are with the Centre for Applied Research in Electronics, Indian Institute of Technology, Delhi, Hauz Khas, New Delhi-110016, India.

0018-9480/83/1200-1051$01.00 ©1983 IEEE

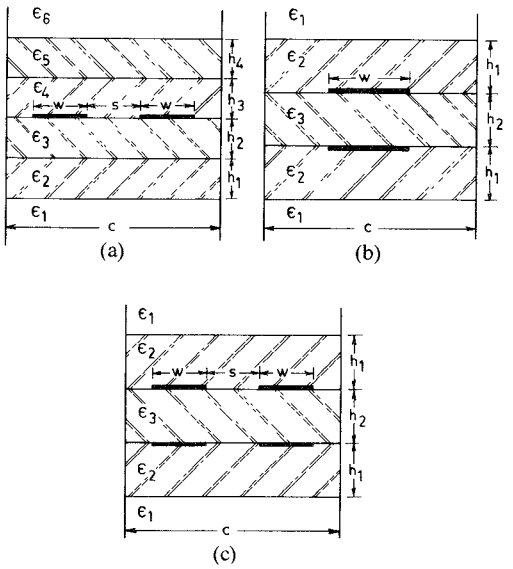

Fig. 2. A schematic of (a) coplanar strip transmission line, (b) broadside-coupled strip transmission line, and (c) coupled coplanar strip transmission line.

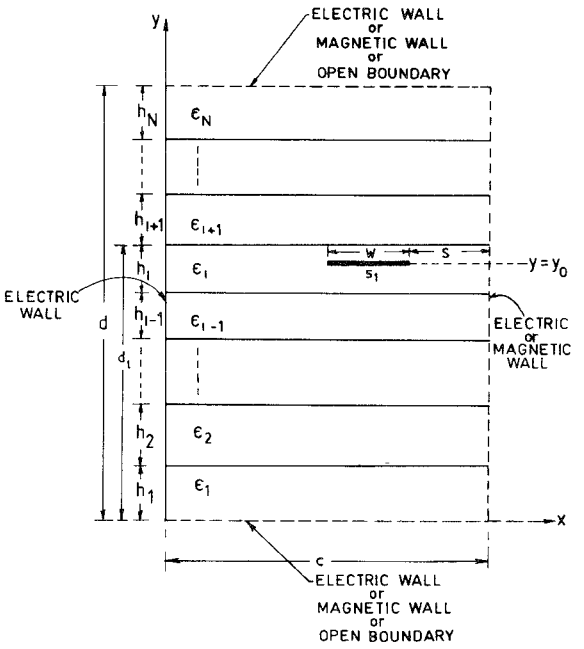

Fig. 3. Cross section of multilayer anisotropic offset single conductor structure.

ital transducer reduces to the determination of capacitance of a pair of coplanar strips embedded in multilayer iso/anisotropic dielectrics (Fig. 2(a)). Besides SAW devices, the coplanar strips embedded in multilayer iso/anisotropic dielectrics find application in MIC and electrooptic modulators [11]–[12]. The analysis of coplanar structures for SAW interdigital transducer applications has been reported by Kino *et al.* [13] and Venema *et al.* [10]. The quasi-static analysis of coplanar strips embedded in anisotropic dielectrics, for electrooptic modulator application, has been reported by Yamashita *et al.* [12]. In these papers, the conventional method of determining the potential function by matching the boundary conditions at various dielectric interfaces is used, which becomes increasingly complicated as the number of dielectric layers increase.

The broadside strips and coupled coplanar strips embedded in multilayer anisotropic dielectrics are shown in Figs. 2(b) and (c), respectively. These structures should find application in MIC filters and directional couplers. The analysis and design data on these transmission lines with iso/anisotropic substrates are not reported in the open literature.

This paper presents a simple unified variational expression for the line capacitance of a general, multilayer anisotropic structure. To use this unified variational expression for determining the line capacitance of various structures with anisotropic substrates having aligned/tilted optical axis, for MIC electrooptic modulator, and SAW IDT applications, it is only necessary to determine the admittance parameter for the particular structure. This admittance parameter can be obtained from the transmission-line equivalent circuit almost by inspection.

II. Analysis

For generality of analysis, using electric and magnetic walls at the planes of symmetry, the transmission lines shown in Figs. 1 and 2 can be represented by a single structure with multilayer dielectrics as shown in Fig. 3. We consider the mode of propagation to be quasi-static. The line capacitance of this structure with anisotropic dielectric substrates can be determined using the variational expression in the space domain [14].

$$C = \frac{\left[\int_{S_1} f(x)\,dx\right]^2}{\int_{S_1}\int_{S_1} G(x, y_0/x_0, y_0) f(x) f(x_0)\,dx\,dx_0}. \quad (1)$$

Here, $f(x)$ is the charge distribution on the conductor strip S_1, and $G(x, y_0/x_0, y_0)$ is the Green's function at the charge plane $y = y_0$. This Green's function satisfies the Poisson's differential equation in the anisotropic media

$$\nabla[\epsilon_i \cdot \nabla G] = -\delta(x - x_0)\delta(y - y_0). \quad (2)$$

$\delta(x - x_0)$ and $\delta(y - y_0)$ are the Dirac's delta functions and ϵ_i is the permittivity tensor of the ith anisotropic dielectric substrate. Determination of the Green's function at the charge plane depends on the type of boundary walls at $x = 0$, $x = c$, $y = 0$, and $y = d$, and also the permittivity tensor ϵ_i of the dielectric substrate. Three different types of permittivity tensors of the dielectric media are considered here.

Case 1

$$\epsilon_i = \epsilon_0 \begin{bmatrix} \epsilon_{xi} & 0 & 0 \\ 0 & \epsilon_{yi} & 0 \\ 0 & 0 & \epsilon_{zi} \end{bmatrix}. \quad (3)$$

The Poisson's equation (2) for this type of dielectric anisotropy can be written as

$$\epsilon_{xi}\frac{\partial^2 G}{\partial x^2} + \epsilon_{yi}\frac{\partial^2 G}{\partial y^2} = -\frac{1}{\epsilon_0}\delta(x - x_0)\delta(y - y_0). \quad (4)$$

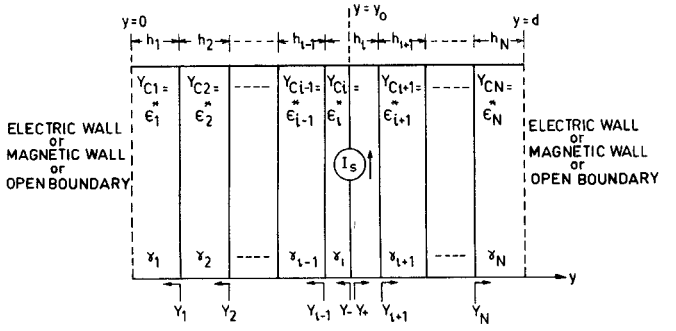

Fig. 4. Transmission-line equivalent of multilayer anisotropic offset single conductor structure.

For the structure under consideration, the Green's function can be expressed as the sum of the product of elementary functions with separated variables

$$G = \sum_n G_n(x) G_n(y). \tag{5}$$

In order to satisfy the boundary conditions on the vertical side walls of the structure shown in Fig. 3, the expression for $G_n(x)$ can be written as

$$G_n(x) = \sin(\alpha_n x) \tag{6a}$$

where

$$\alpha_n = \begin{cases} \dfrac{n\pi}{c}, & n = 1,2,\cdots \text{ for electric wall at } x = c \\ \dfrac{(2n+1)\pi}{2c}, & n = 0,1,\cdots \text{ for magnetic wall at } x = c \end{cases} \tag{6b}$$

Substituting (5) and (6) into (4) and using the orthogonality property of $\sin(n\pi x/c)$ and $\sin((2n+1)\pi x/2c)$ in the interval $(0, c)$, we get

$$\left[\frac{d^2}{dy^2} - \left(\alpha_n \sqrt{\frac{\epsilon_{xi}}{\epsilon_{yi}}}\right)^2\right] G_n(y) = -\frac{2}{c\epsilon_0 \epsilon_{yi}} \delta(y - y_0) \sin(\alpha_n x_0). \tag{7}$$

The Green's function G and, hence, $G_n(y)$ should satisfy the following boundary conditions:

$$G(x, d_i - 0) = G(x, d_i + 0) \tag{8a}$$

$$\epsilon_0 \epsilon_{yi} \frac{\partial}{\partial y} G(x, d_i - 0) = \epsilon_0 \epsilon_{yi+1} \frac{\partial}{\partial y} G(x, d_i + 0), \quad i = 1, \cdots N-1 \tag{8b}$$

Consider a transmission line extending along the y-direction with a current source I_s at $y = y_0$ (Fig. 4). If the transmission line consists of N number of sections cascaded together ($Y_{ci} (= \epsilon_i^*)$ and γ_i being the characteristic admittance and propagation constant of the ith section, respectively), the differential equation satisfied by the voltage along the line is given by

$$\left[\frac{d^2}{dy^2} - \gamma_i^2\right] V = -\left(\frac{\gamma_i}{Y_{ci}}\right) I_s \delta(y - y_0). \tag{9}$$

The continuity conditions at the interfaces between two different sections of the transmission line are given by

$$V_i = V_{i+1} \tag{10a}$$

$$\frac{Y_{ci}}{\gamma_i} \frac{dV_i}{dy} = \frac{Y_{ci+1}}{\gamma_{i+1}} \frac{dV_{i+1}}{dy}, \quad i = 1, \cdots N-1. \tag{10b}$$

Scaling α_n in (10b) and comparing (9) and (10) with (7) and (8), respectively, we get

$$V \equiv G_n(y), \quad I_s = \frac{2}{c\alpha_n} \sin(\alpha_n x_0) \tag{11a}$$

and

$$\gamma_i = \alpha_n \sqrt{\frac{\epsilon_{xi}}{\epsilon_{yi}}}, \quad Y_{ci} = \epsilon_0 \sqrt{\epsilon_{xi} \epsilon_{yi}}. \tag{11b}$$

Since voltage on the transmission line at the charge plane $y = y_0$ is given by $V = I_s/Y$, $Y = Y_+ + Y_-$ being the admittance at the charge plane, we obtain from (5), (6), and (11)

$$G(x, y_0/x_0, y_0)_{\binom{e}{m}} = \sum_{n\binom{\text{even}}{\text{odd}}} \frac{4}{n\pi Y} \sin\left(\frac{n\pi x}{2c}\right) \sin\left(\frac{n\pi x_0}{2c}\right) \tag{12}$$

where n even excludes the value $n = 0$. The subscripts e and m refer to the electric wall and magnetic wall at $x = c$, respectively. Substituting (12) into (1) and assuming a suitable charge distribution $f(x)$ on the strip conductor [15], we get, after performing the required integration

$$C_{\binom{e}{m}} = \frac{\left[1 + 0.25 A_{\binom{e}{m}}\right]^2}{\sum_{n\binom{\text{even}}{\text{odd}}} \left(L_n + A_{\binom{e}{m}} M_n\right)^2 P_n / Y} \tag{13a}$$

where

$$L_n = \sin(\beta_n w/2) \sin(\beta_n (2c - 2s - w)/2)$$

$$\beta_n = n\pi/2c \tag{13b}$$

$$M_n = (2/\beta_n w)^3 \sin(\beta_n (2c - 2s - w)/2) \cdot \left[3\{(\beta_n w/2)^2 - 2\} \times \cos(\beta_n w/2) + (\beta_n w/2) \cdot \{(\beta_n w/2)^2 - 6\} \sin(\beta_n w/2) + 6\right] \tag{13c}$$

$$P_n = (4/n\pi)(2/\beta_n w)^2 \tag{13d}$$

$$A_{\binom{e}{m}} = -\frac{\sum_{n\binom{\text{even}}{\text{odd}}} (L_n - 4M_n) L_n P_n / Y}{\sum_{n\binom{\text{even}}{\text{odd}}} (L_n - 4M_n) M_n P_n / Y}. \tag{13e}$$

The charge distribution constants A_e and A_m [15] given by (13e) have been obtained by maximizing the line capacitances C_e and C_m, respectively (i.e., by setting $(\partial C_e/\partial A_e) = 0$ and $(\partial C_m/\partial A_m) = 0$). These constants are, therefore, named as optimum charge distribution constants.

The only unknown parameter in the above expression is the admittance Y at the charge plane. This parameter can

be obtained from the transmission-line equivalent circuit shown in Fig. 4. The admittance parameter depends on the characteristic admittance Y_c and propagation constant γ of each section of the transmission line and the type of boundary walls at $y=0$ and $y=d$ [16]. For the permittivity tensor of the dielectric substrate given by (3), the characteristic admittances and the propagation constants are given by (11b) with α_n replaced by β_n.

Case 2

$$\epsilon_i = \epsilon_0 \begin{bmatrix} \epsilon_{xxi} & \epsilon_{xyi} & 0 \\ \epsilon_{xyi} & \epsilon_{yyi} & 0 \\ 0 & 0 & \epsilon_{zzi} \end{bmatrix}. \tag{14}$$

Using the approach presented in [17], it can be shown that the capacitance expression (13) is still valid with a modified admittance parameter, which can be obtained from the transmission-line equivalent circuit shown in Fig. 4. For the permittivity tensor of the dielectric substrates given by (14), the characteristic admittances and propagation constants of each section of the transmission line in the equivalent circuit turn out to be

$$Y_{ci} = \epsilon_i^* = \epsilon_0 \sqrt{\epsilon_{xxi}\epsilon_{yyi} - \epsilon_{xyi}^2}, \quad \gamma_i = \beta_n \sqrt{\frac{\epsilon_{xxi}}{\epsilon_{yyi}} - \left[\frac{\epsilon_{xyi}}{\epsilon_{yyi}}\right]^2}, \quad i = 1, \cdots N. \tag{15}$$

Case 3

$$\epsilon_i = \epsilon_0 \begin{bmatrix} \epsilon_{\xi i} & 0 & 0 \\ 0 & \epsilon_{\eta i} & 0 \\ 0 & 0 & \epsilon_{zi} \end{bmatrix}. \tag{16}$$

$\epsilon_{\xi i}$ and $\epsilon_{\eta i}$ are the principal axes relative dielectric constants of the ith anisotropic dielectric substrate. $\xi-\eta$ coordinate system is obtained by rotating $x-y$ coordinate system by an angle θ in the counterclock wise direction. The tensor for the $x-y-z$ coordinate system can be obtained by rotating the principal axes of the ith anisotropic dielectric substrate by an angle θ_i. Using this coordinate transformation, we have

$$\epsilon_i = \epsilon_0 \begin{bmatrix} \epsilon_{\xi i}\cos^2\theta_i + \epsilon_{\eta i}\sin^2\theta_i & -(\epsilon_{\xi i} - \epsilon_{\eta i})\sin\theta_i\cos\theta_i & 0 \\ -(\epsilon_{\xi i} - \epsilon_{\eta i})\sin\theta_i\cos\theta_i & \epsilon_{\eta i}\cos^2\theta_i + \epsilon_{\xi i}\sin^2\theta_i & 0 \\ 0 & 0 & \epsilon_{zi} \end{bmatrix}. \tag{17}$$

The permittivity tensor given by (17) is similar to the tensor given by (14). Therefore, the capacitance expression (13) is still valid with a modified admittance expression, which can be obtained from the transmission-line equivalent circuit shown in Fig. 4. The characteristic admittance and the propagation constant of each section of the transmission line in the equivalent circuit are obtained by comparing (14) and (17) and using (15). These expressions turn out to be

$$Y_{ci} = \epsilon_i^* = \epsilon_0 \sqrt{\epsilon_{\xi i}\epsilon_{\eta i}}$$

$$\gamma_i = \left[\sqrt{\epsilon_{\eta i}/\epsilon_{\xi i}}\right]\left[\left((\epsilon_{\eta i}/\epsilon_{\xi i}) - 1\right)\cos^2\theta_i + 1\right]^{-1}\beta_n, \quad i = 1, \cdots, N. \tag{18}$$

III. Computed Results

The propagation parameters (namely, the characteristic impedance, effective dielectric constant, and phase velocity of a variety of planar transmission lines) can be computed by combining (13) with the standard formulas [14]. To compute the line capacitance, the admittance expressions are obtained from the transmission-line equivalent circuit by using appropriate expressions for Y_{ci} and γ_i, depending on the type of dielectric anisotropy. In all the computations, the thickness of the strip conductor is assumed to be zero. Fig. 5(a) shows the variations of characteristic impedance Z and effective dielectric constant ϵ_{eff} as a function of the angle of tilt θ for symmetric stripline ($d/b=0$) and offset stripline ($d/b=0.2$). Similar variations for suspended stripline are shown in Fig. 5(b). As θ increases, Z decreases and ϵ_{eff} increases for both the symmetric stripline and the offset stripline. On the other hand, for the suspended stripline, Z increases and ϵ_{eff} decreases with an increase in θ. In Fig. 6, the dotted lines show the variations of Z and ϵ_{eff} as a function of $\epsilon_{\xi 1}$ with $\epsilon_{\eta 1}=3.78$ for double-layer microstrip. On the same graph, the solid lines show the variations of Z and ϵ_{eff} as a function of $\epsilon_{\xi 2}$ with $\epsilon_{\eta 2}=3.78$. In both the cases, the principal axes are assumed to be aligned with the axes of the substrate, i.e., $\theta=0$. For a fixed value of $\epsilon_{\xi 2}$, $\epsilon_{\eta 2}$, and $\epsilon_{\eta 1}$, there is negligible change in Z and ϵ_{eff} as $\epsilon_{\xi 1}$ is increased. This indicates that most of the electric field is in the y-direction in the lower dielectric. For a fixed value of $\epsilon_{\xi 1}$, $\epsilon_{\eta 1}$, and $\epsilon_{\eta 2}$, Z decreases and ϵ_{eff} increases with an increase in $\epsilon_{\xi 2}$.

The variations of the even- and odd-mode impedances (Z_{oe}, Z_{oo}) and phase velocity ratio (v_{oe}/v_{oo}) as a function of the angle of tilt θ for symmetric edge-coupled stripline ($d/b=0$) and offset edge-coupled stripline ($d/b=0.2$) are illustrated in Fig. 7. The even- and odd-modes refer to a magnetic and electric wall at $x=c/2$, respectively. It is observed that in both these cases, the phase velocities can be equalized by varying the angle of tilt θ. The variations of v_{oe}/v_{oo} as a function of the anisotropy ratio $\epsilon_\xi/\epsilon_\eta$ with the angle of tilt θ as a parameter are plotted in Fig. 8 for the edge-coupled microstrip. The anisotropy ratio $\epsilon_\xi/\epsilon_\eta$ is normalized with $\epsilon_\eta = 3.78$. It is observed that the two phase velocities can be equalized by a suitable choice of the angle of tilt θ and the anisotropy ratio $\epsilon_\xi/\epsilon_\eta$.

Fig. 9(a) illustrates the variations of the even- and odd-mode impedances (Z_{oe}, Z_{oo}) and the effective dielectric constants (ϵ_{oe}, ϵ_{oo}) as a function of the angle of tilt θ, for the broadside-coupled stripline. The even- and odd-modes refer to a magnetic and electric wall at $y=b/2$, respectively. As θ increases, both Z_{oe} and Z_{oo} decrease, whereas ϵ_{oe} and ϵ_{oo} increase. It is observed that the effective dielectric constants and, hence, the phase velocities can be

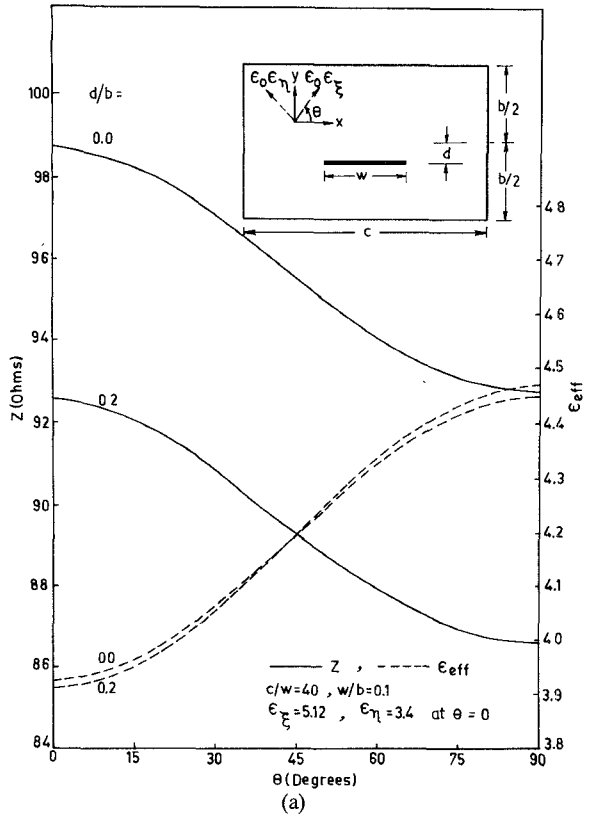

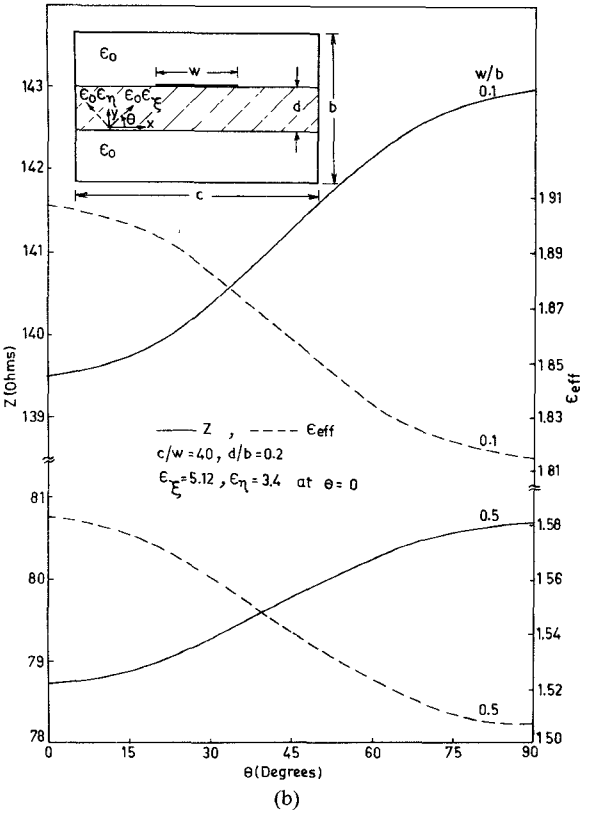

Fig. 5. Characteristic impedance Z and effective dielectric constant ϵ_{eff} versus angle of tilt θ for (a) stripline and (b) suspended stripline.

equalized by varying the angle of tilt θ. Fig. 9(b) illustrates the variations of Z_{oe}, Z_{oo}, ϵ_{oe}, and ϵ_{oo} as a function of the angle of tilt θ for the broadside-coupled microstrip with inverted dielectric. It is observed that Z_{oe} and ϵ_{oo} increase,

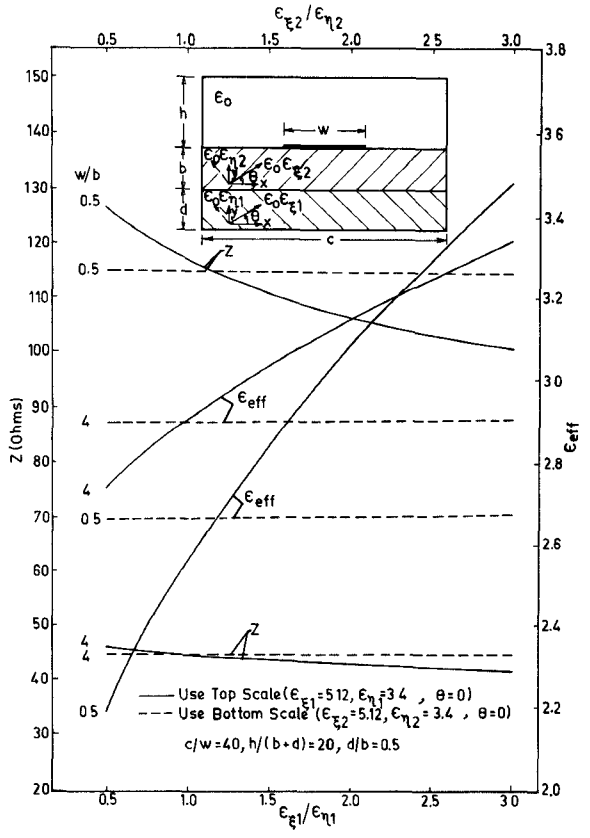

Fig. 6. Characteristic impedance Z and effective dielectric constant ϵ_{eff} versus anisotropy ratio of top and bottom dielectric substrates for double-layer microstrip line.

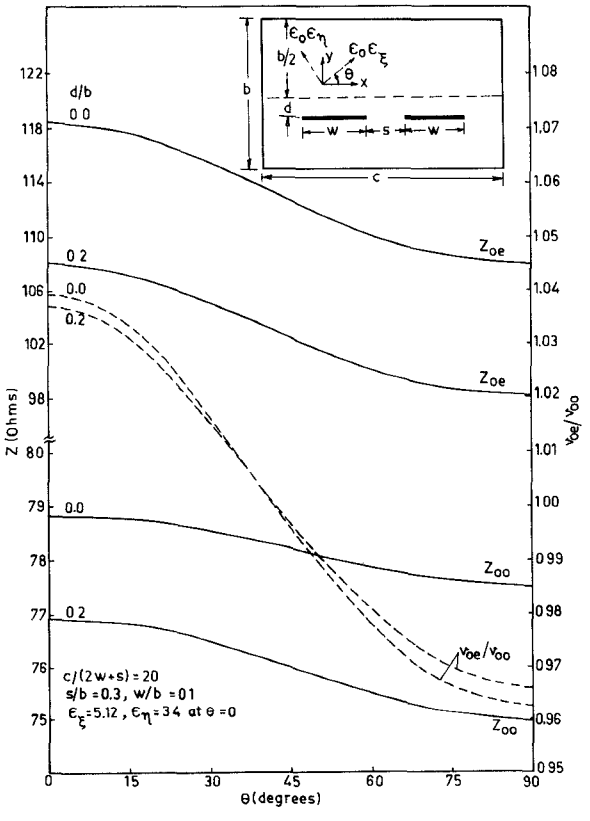

Fig. 7. Even- and odd-mode characteristic impedances (Z_{oe}, Z_{oo}) and phase velocity ratio (v_{oe}/v_{oo}) versus angle of tilt θ for edge-coupled stripline.

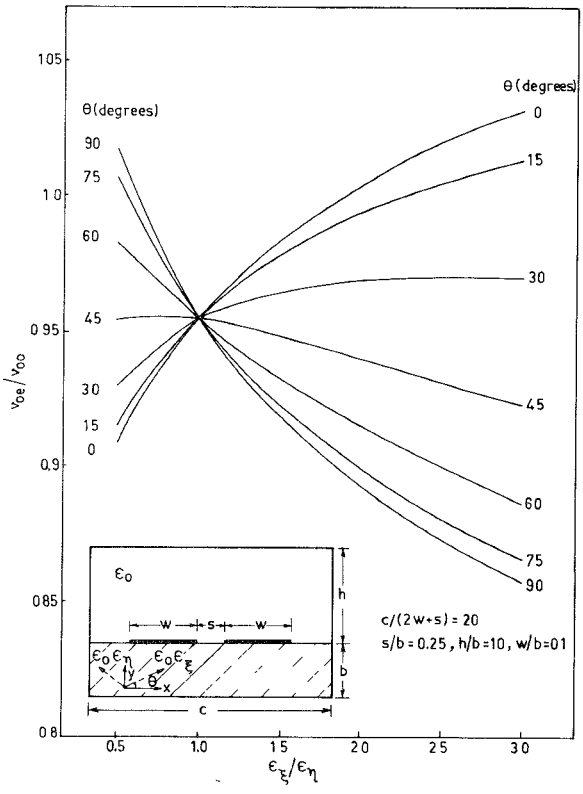

Fig. 8. Phase velocity ratio (v_{oe}/v_{oo}) versus anisotropy ratio ($\epsilon_\xi/\epsilon_\eta$) of the dielectric substrate with angle of tilt θ as a parameter for edge-coupled microstrip.

whereas Z_{oo} and ϵ_{oe} decrease as θ is increased. Therefore, the phase velocity ratio increases as θ increases. This large phase velocity ratio should be useful in designing high-directivity forward-wave directional couplers [18].

The variations of even–even, odd–even, even–odd, and odd–odd mode impedances ($Z_{ee}, Z_{oe}, Z_{eo}, Z_{oo}$) and the corresponding effective dielectric constants ($\epsilon_{ee}, \epsilon_{oe}, \epsilon_{eo}, \epsilon_{oo}$) as a function of anisotropy ratio $\epsilon_\xi/\epsilon_\eta$ normalized with $\epsilon_\eta = 3.78$ are plotted in Fig. 10 for broadside, edge-coupled microstrip. The substrates are assumed to have the principal axes aligned with the axes of the substrate, i.e., $\theta = 0$. The even–even, odd–even, even–odd, and odd–odd modes refer to magnetic walls at $x = c/2$ and $y = b/2$, electric wall at $x = c/2$ and magnetic wall $y = b/2$, magnetic wall at $x = c/2$ and electric wall at $y = b/2$, and electric walls at $x = c/2$ and $y = b/2$, respectively. It is observed from Fig. 10 that all the four impedances decrease, whereas the effective dielectric constants increase as $\epsilon_\xi/\epsilon_\eta$ increases. It may be noted that while using (13) for edge-coupled and broadside edge-coupled structures, c is to be replaced by $c/2$ and s by $s/2$.

The interelectrode capacitances of a coplanar structure for electrooptic modulator applications are plotted in Fig. 11 as a function of the electrode spacing s, for a fixed value of electrode width w. Superimposed on this graph is the variation of capacitance as a function of w, for a fixed value of s. The substrate considered is $LiNbo_3$ having principal axes aligned with the axes of the substrate. For a fixed value of $b = 2$ mm, $w = s = 40$ μm, the capacitance

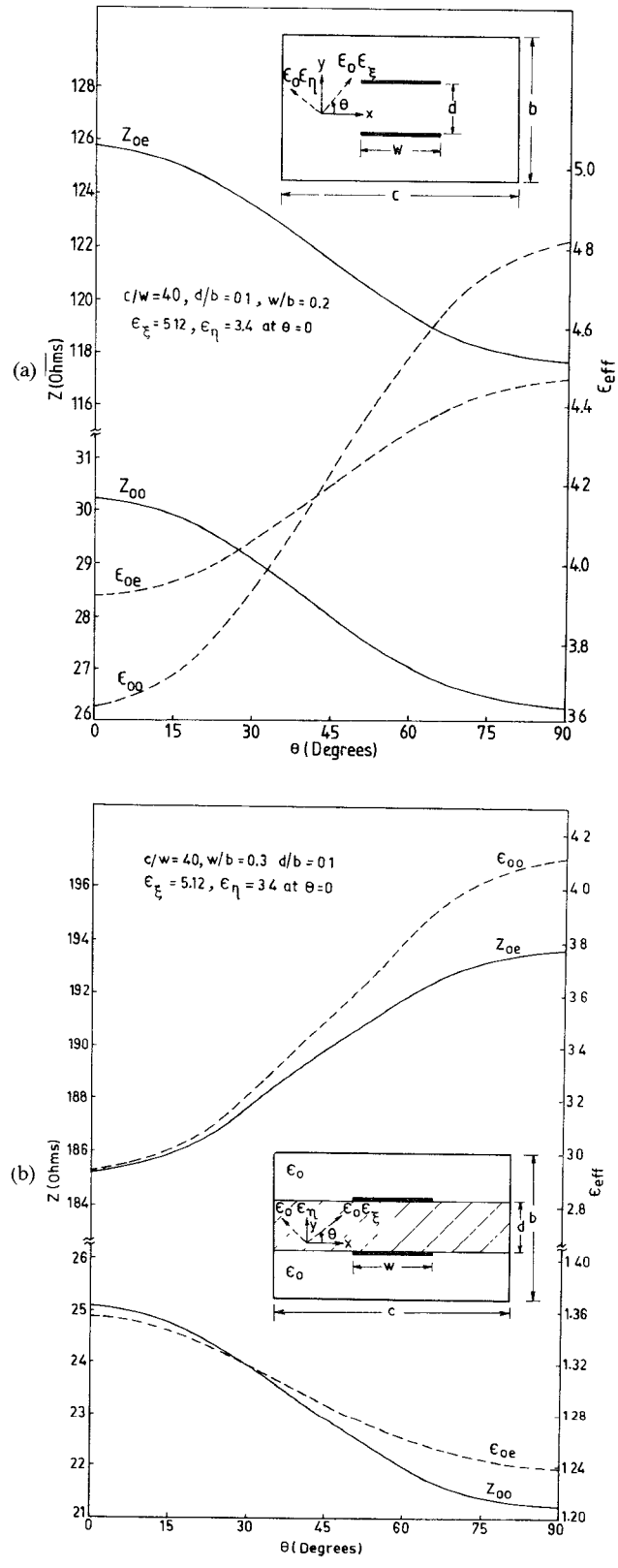

Fig. 9. Even- and odd-mode characteristic impedances (Z_{oe}, Z_{oo}) and effective dielectric constants ($\epsilon_{oe}, \epsilon_{oo}$) versus angle of tilt θ for (a) broadside-coupled stripline and (b) broadside-coupled microstrip with inverted dielectric.

obtained using the present theory is 2.4 PF/cm. This is in good agreement with the value reported (2.44 PF/cm) by Yamashita *et al.* [12].

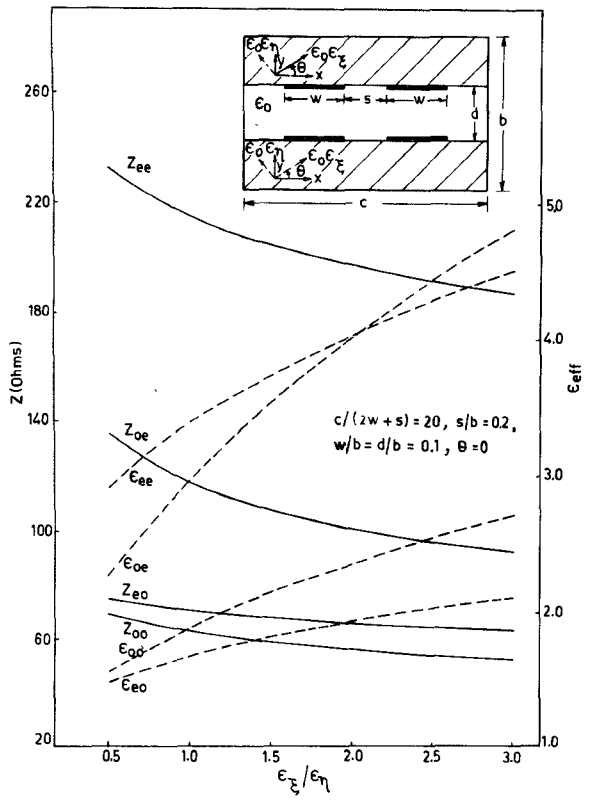

Fig. 10. Even–even, even–odd, odd–even, and odd–odd mode characteristic impedances ($Z_{ee}, Z_{eo}, Z_{oe}, Z_{oo}$) and effective dielectric constants ($\epsilon_{ee}, \epsilon_{eo}, \epsilon_{oe}, \epsilon_{oo}$) versus anisotropy ratio ($\epsilon_\xi/\epsilon_\eta$) of the dielectric substrate for broadside, edge-coupled microstrip.

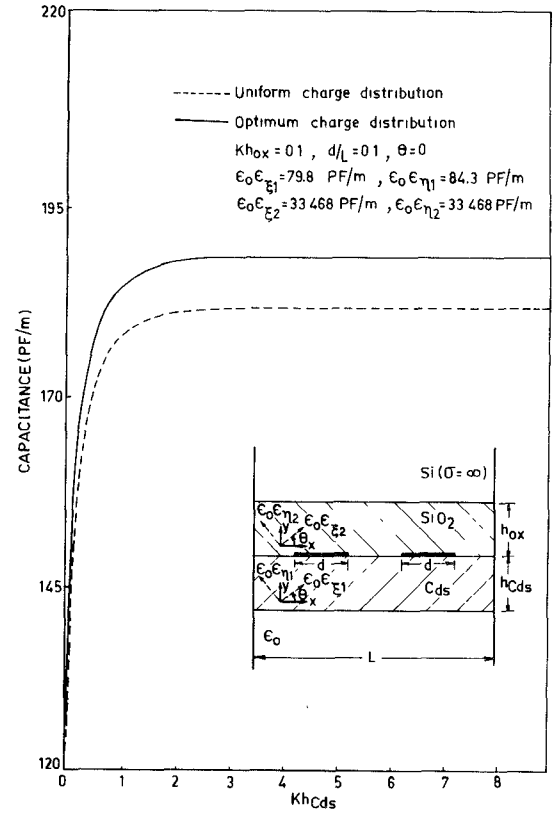

Fig. 12. Variation of static capacitance of Cds–SiO_2–Si SAW structure using uniform and optimum charge distributions versus normalized height of the Cds layer.

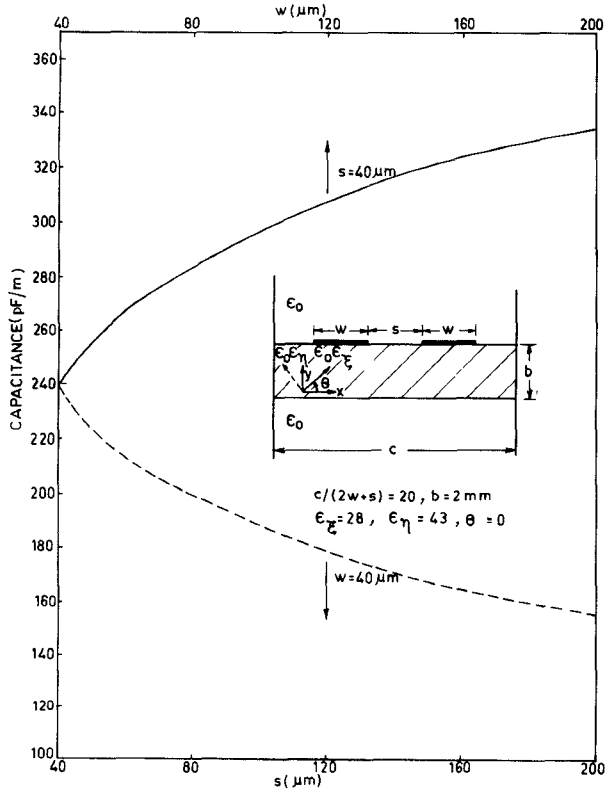

Fig. 11. Variation of interelectrode capacitance of coplanar structure for electrooptic modulator versus width w of the electrodes and spacing s between the electrodes.

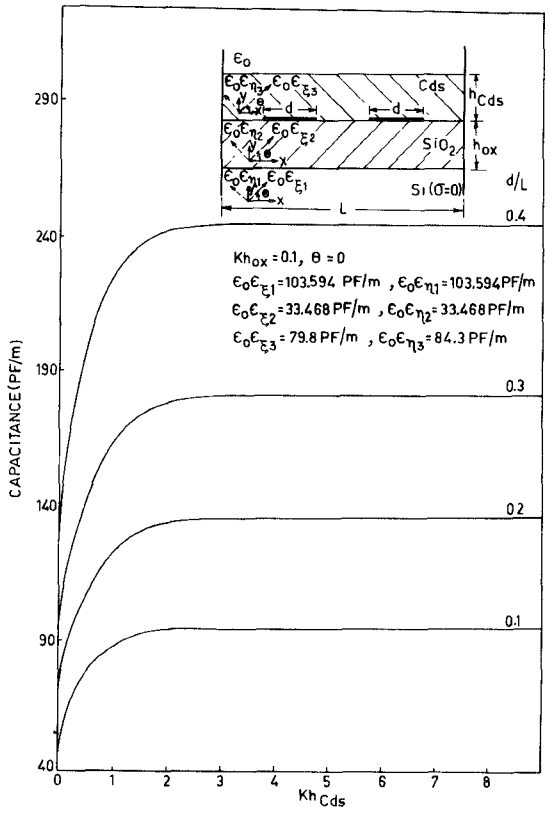

Fig. 13. Static capacitance of Cds–SiO_2–Si SAW structure versus normalized height of the Cds layer with d/L as the parameter.

The static capacitances of a typical Cds–Sio_2–Si SAW structure as a function of the normalized height of the Cds layer are plotted in Fig. 12 using the uniform charge distribution ($A = 0$ in our theory) and also the optimum charge distribution [5], [14]. The normalizing factor is $K = 2\pi/L$. The capacitance values obtained using the optimum charge distribution are higher than those obtained with the uniform charge distribution. Since the capacitance expression (13) is variational, a charge distribution which maximizes the line capacitance yields more accurate results than the uniform charge distribution.

The analysis and numerical results presented in [10] use the uniform charge distribution on the electrodes. Fig. 13 illustrates the variations of the capacitance of Cds–SiO_2–Si SAW structure as a function of the normalized height of the Cds layer with d/L as a parameter. The normalizing factor $K = 2\pi/L$. These capacitance values are computed using the optimum charge distribution.

IV. Conclusions

A unified variational expression for determining the line capacitance of various microstrip-like transmission lines and coplanar strips with anisotropic substrates for MIC, electrooptic modulators, and SAW IDT is given in this paper. Using the formulas presented, the study of propagation characteristics of a variety of structures with anisotropic substrates having an aligned/tilted optical axis reduces to the determination of a single admittance parameter. The characteristics of symmetric stripline, offset stripline, suspended stripline, and double-layer microstrip with anisotropic substrates were presented. It is shown that the even- and odd-mode phase velocities in the case of edge-coupled stripline, edge-coupled microstripline, and broadside-coupled stripline can be equalized by varying the angle of tilt θ. For the broadside-coupled microstrip with inverted dielectric, the phase velocity ratio can be increased by varying the angle of tilt θ. This increase in phase velocity ratio should be useful in designing high-directivity forward-wave couplers. The characteristics of the coplanar structure for electrooptic modulator applications are analyzed. More accurate results on the static capacitance of Cds–SiO_2–Si SAW IDT using the optimum charge distribution on the electrodes are presented.

References

[1] Ingo Wolff, MIC-Bibliography, Aachen, Germany, 1979.

[2] R. P. Owens, J. E. Aitken, and T. C. Edwards, "Quasi-static characteristics of microstrip on an anisotropic sapphire substrate," *IEEE Trans. Microwave Theory Tech.*, vol. MTT-24, pp. 499–505, Aug. 1976.

[3] C. M. Krowne, "Microstrip transmission lines on pyrolytic boron nitride," *Electron. Lett.*, vol. 12, pp. 642–643, Nov. 1976.

[4] A. G. d'Assuncao, A. J. Giarola, and D. A. Rogers, "Analysis of single and coupled striplines with anisotropic substrates," in *IEEE MTT-S 1981 Int. Microwave Symp. Dig.* (Los Angeles, CA), June, 1981, pp. 83–85.

[5] S. K. Koul and B. Bhat, "Transverse transmission line method for the analysis of broadside-coupled microstrip lines with anisotropic substrates," *Arch. Elek. Ubertragung.*, vol. 37, pp. 59–64, Jan/Feb. 1983.

[6] H. Shibata, S. Minakawa, and R. Terakado, "Analysis of the shielded-strip transmission line with an anisotropic medium," *IEEE Trans. Microwave Theory Tech.*, vol. MTT-30, pp. 1264–1267, Aug. 1982.

[7] N. G. Alexopoulos and S. A. Maas, "Characteristics of microstrip directional couplers on anisotropic substrates," *IEEE Trans. Microwave Theory Tech.*, vol. MTT-30, pp. 1267–1270, Aug. 1982.

[8] S. K. Koul and B. Bhat, "Inverted microstrip and suspended microstrip with anisotropic substrates," *Proc. IEEE*, vol. 70, pp. 1230–1231, Oct. 1982.

[9] S. K. Koul and B. Bhat, "Shielded edge-coupled microstrip structure with anisotropic substrates," *Arch. Elek. Übertragung.*, vol. 37, pp. 269–274, July/Aug. 1983.

[10] A. Venema, J. M. Dekkers, and R. F. Humphryes, "Static capacitance calculations for a surface acoustic wave interdigital transducer in multilayered media," *IEEE Trans. Microwave Theory Tech.*, vol. MTT-26, pp. 294–297, Apr. 1978.

[11] J. B. Knorr and K. Kuchler, "Analysis of coupled slots and coplanar strips on dielectric substrate," *IEEE Trans. Microwave Theory Tech.*, vol. MTT-23, pp. 541–548, July 1975.

[12] E. Yamashita, K. Atsuki, and T. Mori, "Application of MIC formulas to a class of integrated-optics modulator analysis: A simple transformation," *IEEE Trans. Microwave Theory Tech.*, vol. MTT-25, pp. 146–150, Feb. 1977.

[13] G. S. Kino and R. S. Wagers, "Theory of interdigital couplers on nonpiezoelectric substrates," *J. Appl. Phys.*, vol. 44, no. 4, pp. 1480–1488, Apr. 1973.

[14] R. E. Collin, *Field Theory of Guided Waves*. New York: McGraw Hill, 1960.

[15] S. K. Koul and B. Bhat, "Characteristics of shielded double layer microstrip for high directivity coupler applications," *Arch. Elek. Übertragung.*, vol. 36, pp. 207–212, May 1982.

[16] B. Bhat and S. K. Koul, "Unified approach to solve a class of strip and microstrip-like transmission lines," *IEEE Trans. Microwave Theory Tech.*, vol. MTT-30, pp. 679–685, May 1982.

[17] B. Bhat and S. K. Koul, "A new approach to analyse microstrip-like transmission lines with anisotropic substrates having tilted optical axis," submitted to *Proc. Inst. Elec. Eng., Microwaves, Optics and Antennas (MOA)*, part H.

[18] J. E. Dalley, "A stripline directional coupler utilizing a nonhomogeneous dielectric medium," *IEEE Trans. Microwave Theory Tech.*, vol. MTT-17, pp. 706–712, Sept. 1969.

Shiban Kishen Koul (S'81) received the B.E. degree in electrical engineering from the Regional Engineering College, Srinagar, J&K, India, in 1977, and the M.Tech. degree in radar and communication engineering with distinction from the Indian Institute of Technology (IIT), Delhi, India, in 1979.

From 1979 to 1980, he worked as a Senior Research Assistant in the Centre for Applied Research in Electronics (CARE) at the Indian Institute of Technology, Delhi. Since 1980, he has been a Senior Scientific Officer in CARE. He entered the Ph.D. program as a part-time student, in January 1980, and has just submitted his thesis in the area of microstrip-like transmission lines. He is presently engaged in research in the areas of thin film microwave integrated circuits, ferrite phase shifters, and millimeter-wave transmission lines.

Mr. Koul is currently the Joint Secretary of the IEEE ED/MTT Chapter of the IEEE India Council. He was awarded a Gold Medal by the Institution of Engineers (India) for securing first position among all the disciplines of Engineering in the B.E. degree course.

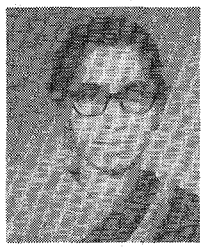

Bharathi Bhat (SM'82) received the B.E. degree in electrical communication engineering and the M.E. degree in electronics both with distinction from the Indian Institute of Science, Bangalore, India, in 1963 and 1965, respectively. She continued her graduate studies at Harvard University, Cambridge, MA, and received the M.S. and Ph.D. degrees from the Division of Engineering and Applied Physics in 1967 and 1971, respectively.

From 1971 to 1972, she worked as a Post-Doc-

toral Research Fellow in the Division of Engineering and Applied Physics, Harvard University. In 1973, she joined the Indian Institute of Technology, New Delhi, as Assistant Professor. Since 1977, she has been a Professor at the Centre for Applied Research in Electronics (CARE). During the period 1979–1982, she was the Head of CARE, IIT, New Delhi. She is also the leader of the Microwave Group in CARE and has been directing a number of sponsored research projects in the areas of microwave antennas, electronic phase shifters, and microwave and millimeter-wave integrated circuits and components.

Dr. Bhat is a Fellow of the Institution of Electronics and Telecommunication Engineers (IETE), India. She has been the Honorary Editor of the IETE Journal (electromagnetics section) since January 1981 and a member of the IETE Council since January 1982. She is presently the Chairman of the ED/MTT Chapter of the IEEE India Council.

Loop-Gap Resonator: A Lumped Mode Microwave Resonant Structure

MEHRDAD MEHDIZADEH, STUDENT MEMBER, IEEE, T. KORYU ISHII, SENIOR MEMBER, IEEE, JAMES S. HYDE, AND WOJCIECH FRONCISZ

Abstract—**Loop-gap resonators are newly developed microwave resonant structures with a field configuration that is intermediate between lumped and distributed. Typical characteristic dimensions are of the order of 1/10 of the resonant wavelength, and typical Q's are of the order of 1600–2000 in the frequency range of 1–4 GHz. Data are presented for Q's and frequencies for a series of resonators of various dimensions and compared with theory. Various coupling and frequency tuning techniques are discussed, and results of experiments are reported. Results of preliminary application of the structure in microwave filters and oscillators are presented. Loop-gap resonators provide a useful design alternative, it is concluded, to dielectric and surface acoustic-wave resonators at low microwave frequencies.**

I. Introduction and General Description of the Resonator

AT LOW FREQUENCY microwave bands of L and S, the choice of resonators presents a problem because of the large size of resonant cavities and the high loss of lumped-element circuits. Miniature lumped-element resonant circuits were described in [1], which are composed of an interdigital capacitor and a loop inductor etched on an MIC substrate. They were designed for X-band frequencies with a Q of about 700. Here we describe a resonant structure with a lumped-mode field configuration where the transmission line between the inductive and capacitive elements is eliminated; therefore, these elements are in juxtaposition which results in low loss.

Manuscript received April 19, 1983; revised August 4, 1983. This work was supported in part by Grants RR01008 and GM27665 from the National Institutes of Health.

M. Mehdizadeh and T. K. Ishii are with the Department of Electrical Engineering and Computer Science, Marquette University, Milwaukee, WI 53233.

J. S. Hyde and M. Mehdizadeh are with the National Biomedical ESR Center, Department of Radiology, Medical College of Wisconsin, Milwaukee, WI 53226.

W. Froncisz is currently with the Medical College of Wisconsin, on leave from the Institute of Molecular Biology, Jagiellonian University, Kracow, Poland.

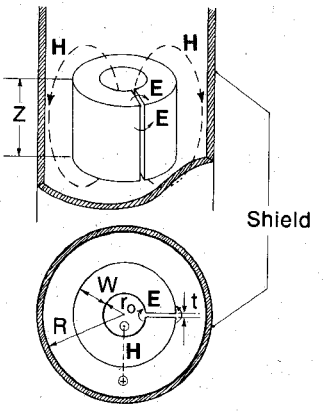

Fig. 1. The loop-gap resonator and cross-sectional view.

The loop-gap resonator is shown in Fig. 1. It consists of a conductive cylindrical loop cut by one or more longitudinal slots (or gaps). In this paper, only single-gap resonators are discussed. The structure is shielded by a conductive cylinder coaxial with the resonator. The resonators discussed here are machined from brass stock and silver plated for better Q. The resonator is supported in position within the cylindrical shield by the use of a semi-annular piece of Rexolite and plastic screws.

The electric fields, as shown in Fig. 1, are supported by the gap with the magnetic fields surrounding the loop. The conduction current, which flows in a circumferential direction on surfaces of the loop, transforms into displacement current in the gap.

0018-9480/83/1200-1059$01.00 ©1983 IEEE